

Observation of field-induced reverse transformation in ferromagnetic shape memory alloy $\text{Ni}_{50}\text{Mn}_{36}\text{Sn}_{14}$

Keiichi Koyama^{a)} and Kazuo Watanabe

High Field Laboratory for Superconducting Materials, Institute for Materials Research, Tohoku University, Sendai 980-8577, Japan

Takeshi Kanomata

Faculty of Engineering, Tohoku Gakuin University, Tagajyo 985-8537, Japan

Ryosuke Kainuma, Katsunari Oikawa, and Kiyohito Ishida

Department of Materials Science, Graduate School of Engineering, Tohoku University, Sendai 980-8571, Japan

(Received 29 December 2005; accepted 12 February 2006; published online 27 March 2006)

The structural and magnetic properties of the ferromagnetic Heusler alloy $\text{Ni}_{50}\text{Mn}_{36}\text{Sn}_{14}$ were studied by magnetization and x-ray powder diffraction measurements in fields up to 5 T. The alloy undergoes the martensitic transformation from the $L2_1$ -type cubic structure with the lattice parameter $a_c=0.5988$ nm into an orthorhombic structure with the lattice parameters $a_o=0.8617$ nm, $b_o=0.5702$ nm and $c_o=0.4359$ nm at $M_s=220$ K with a thermal hysteresis of 40 K. The cell volume contracts by 0.37% and the magnetic moment decreases by 50% at M_s . Furthermore, we directly observed the field-induced reverse martensitic transformation. © 2006 American Institute of Physics. [DOI: 10.1063/1.2189916]

Ternary intermetallic compound Ni_2MnSn is a ferromagnet with the Curie temperature of $T_C \sim 340$ K.¹⁻⁵ The compound is one of Heusler alloys, which has the cubic $L2_1$ -type ($L2_1$) structure. In this structure, the Ni ions occupy at the site of the cube corners (8c-site), and Mn and Sn ions are in the alternate body centers of the successive cubes (4a- and 4c-sites, respectively). It had been not reported for the structural transformation in the stoichiometric compound Ni_2MnSn . Recently, however, Suto *et al.* found that the ferromagnetic Heusler alloys $\text{Ni}_{50}\text{Mn}_{50-y}\text{X}_y$ ($X=\text{In, Sn, and Sb}$) show the martensitic transformation from the $L2_1$ structure to an orthorhombic four-layered (4O) structure in the ferromagnetic state.⁶ Their results indicate that the $\text{Ni}_{50}\text{Mn}_{50-y}\text{X}_y$ alloy will exhibit field-induced magnetic and structural transitions such as those of Ni_2MnGa ,⁷⁻⁹ which are so-called “ferromagnetic shape-memory alloys” (FMSAs). However, it was supposed that the magnetic moment in the low temperature (LT) phase (m_L) is smaller than that in the high temperature (HT) phase (m_H) in $\text{Ni}_{50}\text{Mn}_{50-y}\text{X}_y$.^{6,10,11} This is different from Ni_2MnGa , which has the higher magnetic moment in the LT-phase, compared with that in the HT phase. Therefore, it is very important to reveal the structural and magnetic properties of the $\text{Ni}_{50}\text{Mn}_{50-y}\text{X}_y$ alloy in magnetic fields and to confirm the field-induced structural transformation for development of the new FSMAs.

In this study, in order to clarify a relationship between the structural and magnetic properties for $\text{Ni}_{50}\text{Mn}_{36}\text{Sn}_{14}$ in magnetic fields, we have carried out high-field magnetization and x-ray powder diffraction (XRD) measurements under magnetic fields up to 5 T in the wide temperature ranging from 8 to 300 K.

The polycrystalline sample of $\text{Ni}_{50}\text{Mn}_{36}\text{Sn}_{14}$ has been prepared by induction melting under an argon atmosphere.

The detailed sample preparation was reported in Ref. 6. The obtained sample was confirmed to be a single phase with the $L2_1$ structure by XRD measurements at room temperature. The magnetic transition temperatures were determined by the temperature dependence of the ac initial permeability μ using an ac transformer method. The magnetic moment m was measured using a vibrating sample magnetometer for the powder sample in magnetic fields B up to 13 T at the temperature T ranging from 4 to 300 K. In this measurement, the powder sample was fixed with nonmagnetic wax in a sample holder after measuring the mass. Therefore, the powder was not affected by magnetic alignment in the high-field magnetization process. The XRD experiments with $\text{Cu } K\alpha$ radiation were made at $8.6 \leq T \leq 300$ K in magnetic fields up to 5 T.¹² The powder was fixed with vacuum grease on a copper sample holder. The diffraction data were taken at $20^\circ \leq 2\theta \leq 85^\circ$ with a step size of 0.01° . We confirmed that the powder sample was not removed by the magnetic force until the measurement in high fields was completed.

Figure 1 shows the μ - T curves (a) and the typical m - B curves (b) at 220, 240, and 250 K. Here, these m - B curves are measured after zero-field heating from 100 K. The Curie temperature T_C is determined to be 317 K. As shown in Fig. 1(a), the magnetic phase transitions are seen at the vicinity of 220 K with a hysteresis of approximately 40 K, indicating that a martensitic transformation occurs. From the μ - T curves, the characteristic temperatures M_s , M_f , A_s , and A_f , are determined to be 220, 210, 240, and 250 K, respectively. These values are consistent with the magnetic data reported in Refs. 6, 10, and 11.

At 220 K ($<A_s$), m is $35.5 \text{ A m}^2 \text{ kg}^{-1}$ at 5 T, which is slightly smaller than that ($40.7 \text{ A m}^2 \text{ kg}^{-1}$) at 4 K. On the other hand, m at 250 K is approximately two times larger than that at 220 K and reaches up to $61.0 \text{ A m}^2 \text{ kg}^{-1}$ at 5 T. These values are consistent with the previous reports.^{10,11} For $4 \leq T < 220$ K (LT phase) and $T \geq 250$ K (HT phase), we cannot see any anomaly on the m - B curves in fields up to

^{a)} Author to whom correspondence should be addressed; electronic mail: kkoyama@imr.tohoku.ac.jp

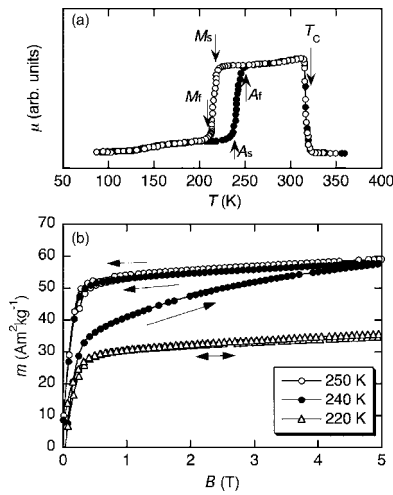


FIG. 1. Temperature dependence of the initial ac permeability (a) and magnetization curves (b) of $\text{Ni}_{50}\text{Mn}_{36}\text{Sn}_{14}$. Vertical arrows in the panel (a) indicate the determined characteristic temperatures T_C , M_S , M_f , A_S , and A_f . The arrows in the panel (b) indicate, the magnetization process with increasing and decreasing fields B . These magnetization curves are measured after zero-field heating from 100 K.

13 T. At $A_S < T < A_f$, a large magnetic hysteresis is observed on the m - B curves. In Fig. 1(b), we show the typical result of the observed magnetic hysteresis at 240 K. In the initial magnetization process, m is $35.0 \text{ A m}^2 \text{ kg}^{-1}$ at 0.5 T, and then it rapidly increases with increasing B . At 5 T, m reaches up to $60.0 \text{ A m}^2 \text{ kg}^{-1}$, which is almost same value at 250 K. The demagnetization process with decreasing B is not traced on the initial magnetization process but the m - B curves at 250 K, and a large hysteresis is exhibited. That is, m in the HT phase (m_H) is larger than that in the LT phase (m_L). In $A_S \leq T \leq A_f$, moreover, a magnetic phase transition from m_L to m_H occurs by applying B , which is an irreversible process.

Figure 2 shows the typical XRD profiles of $\text{Ni}_{50}\text{Mn}_{36}\text{Sn}_{14}$ in $40^\circ \leq 2\theta \leq 44^\circ$ at several temperatures for cooling (a) and heating (b) processes in a zero magnetic field. Here, the reflections by $K\alpha_1$ and $K\alpha_2$ radiations are observed. We confirmed that the HT phase has a $L2_1$ structure. On the other hand, the profiles in the LT phase quite differ from that in the HT phase, indicating that the $L2_1$ structure drastically changes to another one. The results of the transmission electron microscopy measurements by Suto *et al.* suggest that the $L2_1$ structure undergoes the martensitic transformation into an orthorhombic four-layered (4O) structure in $\text{Ni}_{50}\text{Mn}_{50-y}\text{Sn}_y$.⁶ Assuming that the LT phase has the 4O structure, we can index all reflections for $20^\circ \leq 2\theta \leq 85^\circ$. In Fig. 2, hkl_C and hkl_O denote the Miller indices for the $L2_1$ and 4O structures, respectively.

The Bragg peaks of the $L2_1$ structure are only seen above 230 K ($>M_S$) for cooling. With decreasing T from 220 K ($=M_S$), the peaks of the 4O structure appear and develop, and the intensity of the peaks of the $L2_1$ structure becomes smaller. The peak intensity of the 4O structure does not change below 200 K ($<M_f$). As shown in Fig. 2(b), the peak intensity of the 4O structure becomes small above 230 K ($\sim A_S$) with increasing T , and cannot be detected above 250 K ($>A_f$). In contrast, the HT phase with the $L2_1$ structure develops above 230 K and is only observed over 250 K. That is, the fraction of the LT phase decreases between A_S and A_f for heating.

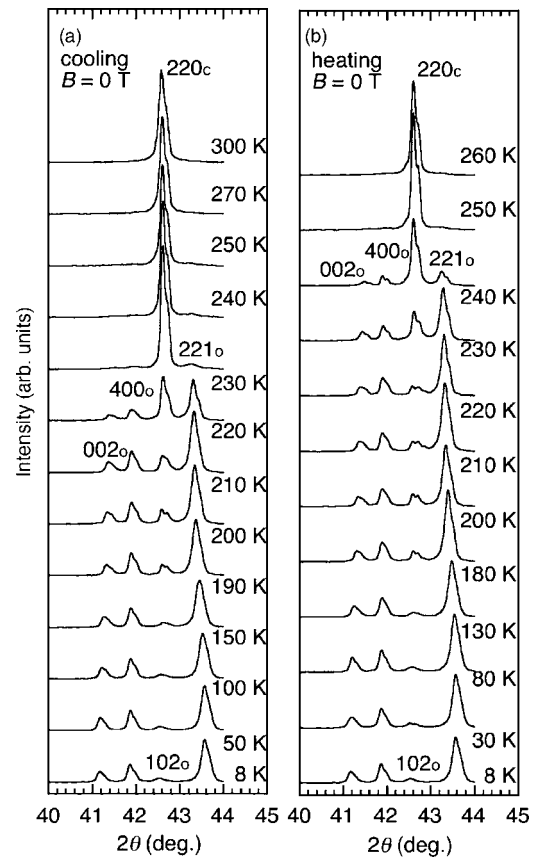


FIG. 2. X-ray powder diffraction profiles of $\text{Ni}_{50}\text{Mn}_{36}\text{Sn}_{14}$ at various temperatures for cooling (a) and heating (b) processes from 310 to 8 K in zero magnetic field. hkl_C and hkl_O denote the Miller indices for the cubic $L2_1$ -type and four-layered orthorhombic (4O) structures, respectively.

Figure 3 shows the temperature dependence of the lattice parameters (a) and the cell volume (b) in a zero field. Here, the parameters (a_c and V_c) and (a_o , b_o , c_o , and V_o) indicate the data for the $L2_1$ and 4O structures, respectively. This 4O structure basically consists of the modulated and four-

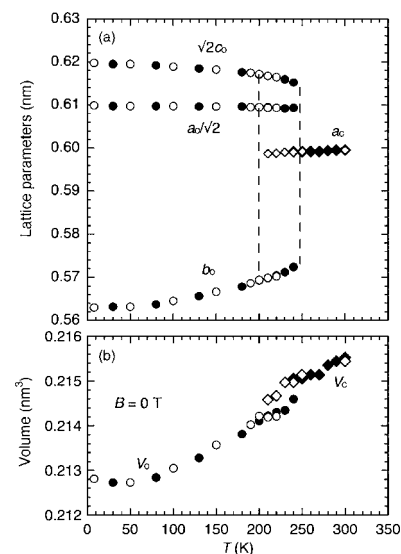


FIG. 3. Temperature dependence of the lattice parameters (a) and the unit cell volumes (b) for $\text{Ni}_{50}\text{Mn}_{36}\text{Sn}_{14}$ in a zero field. The open and closed symbols show the data for heating and cooling processes, respectively. The dashed lines indicate the thermal hysteresis with varying fraction of the four-layered orthorhombic structure (4O) phase among M_S , M_f , A_S , and A_f .

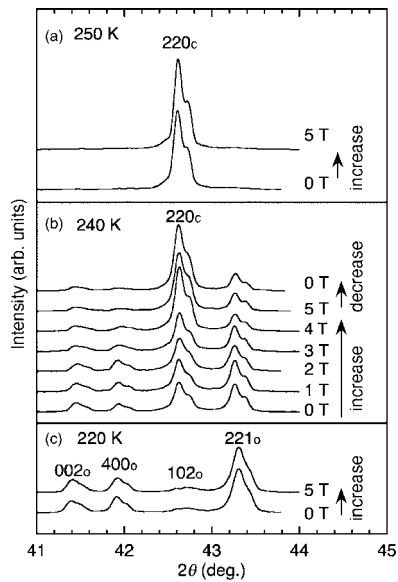


FIG. 4. X-ray powder diffraction profiles of $\text{Ni}_{50}\text{Mn}_{36}\text{Sn}_{14}$ in magnetic fields up to 5 T at 250 K (a), 240 K (b), and 220 K (c). hkl_c and hkl_o denote the Miller for the cubic $L2_1$ -type and four-layered orthorhombic (4O) structures, respectively.

layered $\{220\}$ sheets along the $[221]$ direction of the parent $L2_1$ structure.⁶ Recent result of neutron diffraction measurement by Brown *et al.* suggests that the space group of the 4O structure is $Pmma$.¹³ The axes and volumes of the two structures are related to $a_o = \sqrt{2}a_c$, $b_o = a_c$, $c_o = a_c/\sqrt{2}$ and $V_o = V_c$. The dashed lines in this figure indicate thermal hysteresis considering the peak intensity variation of XRD results between the $L2_1$ HT phase and the 4O LT phase. In the HT phase above M_s , a_c slightly decreases with decreasing T . The thermal expansion coefficients of a_c at 250 K in the HT phase is estimated to be $\alpha_a(L2_1) = 1.3 \times 10^{-5} \text{ K}^{-1}$. The $L2_1$ structure transforms into the 4O structure at $M_f - A_f$. The lattice decreases by 5.3% along the b_o axis at M_f for cooling, while the other lattices increases by 1.7% and 3.0% along the a_o and c_o axes, respectively, leading that the volume contracts by 0.37%. In addition, we found that the temperature dependence of the lattice parameters is very unique in the LT phase. With decreasing T , a_o increases, b_o decreases, and c_o slightly increases. The thermal expansion coefficients of a_o , b_o , and c_o axes at 200 K are estimated to be $\alpha_a(4O) = -0.5 \times 10^{-5} \text{ K}^{-1}$, $\alpha_b(4O) = 9.2 \times 10^{-5} \text{ K}^{-1}$, and $\alpha_c(4O) = -5.7 \times 10^{-5} \text{ K}^{-1}$, respectively.

In Fig. 4, we show the typical results of the XRD profile of $\text{Ni}_{50}\text{Mn}_{36}\text{Sn}_{14}$ in fields up to 5 T at 250 K (a), 240 K (b), and 220 K (c). Here, all field dependence profiles are measured after zero-field heating from 100 K. As shown in Figs. 4(a) and 4(c), the profiles do not drastically change by applying magnetic fields up to 5 T in the $L2_1$ and 4O structures, respectively. We found that the lattice parameters and volumes for both phases are almost independent for B . In contrast, we clearly see the field-induced structural transformation at $A_s \leq T \leq A_f$, as shown in Fig. 4(b). In $B = 0$ T, the profile shows the two-phase coexistence consisting of the LT (4O) and HT ($L2_1$) phases at 240 K. With increasing B , the reflection peak of the LT (4O) phase is suppressed but the peak of the HT ($L2_1$) phase is enhanced, and then the profile

shows almost a single phase of the HT phase at 5 T. In decreasing B , the intensity of the peak of the HT ($L2_1$) phase still remains and the peak of the LT (4O) phase dose not recover down to a zero field. This irreversible process is consistent with the magnetization process with the large hysteresis at 240 K, as shown in Fig. 1(b). That is to say, the results presented clearly show that $\text{Ni}_{50}\text{Mn}_{36}\text{Sn}_{14}$ exhibits the field induced reverse transformation from the 4O structure with the lower m_L to the $L2_1$ structure with the higher m_H . Moreover, we found that a high field over 5 T is required to completely lead the field-induced reverse transformation around A_s .

Assuming the simple ferromagnetic structure in the LT phase, the enhancement of m at A_s is probably due to suppression of the $3d$ - $3d$ overlap, accompanied with the structural transformation from the small V in the LT phase to large V in the HT phase. The observed field-induced reverse transformation from the LT phase with low m_L to HT phase with high m_H probably occurs to decrease the magnetic energy because of the addition of the Zeeman energy. However, in order to understand the contribution of the magnetic properties for the martensitic transformation, it is required to study the detailed magnetic structure and electronic band structure in $\text{Ni}_{50}\text{Mn}_{50-y}\text{X}_y$ ($X = \text{In}$, Sn , and Sb).

In summary, the magnetization and XRD measurements for $\text{Ni}_{50}\text{Mn}_{36}\text{Sn}_{14}$ were carried out in magnetic fields up to 5 T. In this study, we confirmed that the compound exhibits the martensitic transformation from the $L2_1$ structure to 4O structure. The magnetic moment in the 4O LT phase is smaller by 50% than that in the $L2_1$ HT phase. Our results clearly show that the magnetic field induces the reverse transformation in $\text{Ni}_{50}\text{Mn}_{36}\text{Sn}_{14}$ at the vicinity of M_s .

The XRD and magnetization measurements were carried out at the High Field Laboratory for Superconducting Materials, Institute for Materials Research and the Center for Low Temperature Science, Tohoku University, respectively. This work was supported by a Grant in-Aid for Scientific Research from the Ministry of Education, Science and Culture, Sports, Science and Technology of Japan.

¹L. Castelliz, Z. Metallkd. **46**, 198 (1955).

²T. Shinohara, J. Phys. Soc. Jpn. **28**, 313 (1970).

³C. C. M. Campbell, J. Phys. F: Met. Phys. **5**, 1931 (1975).

⁴C. C. M. Campbell and C. V. Stager, Can. J. Phys. **54**, 2197 (1976).

⁵T. Kanomata, K. Shirakawa, and T. Kaneko, J. Magn. Magn. Mater. **65**, 76 (1987).

⁶Y. Suto, Y. Imano, N. Koeda, T. Omori, R. Kainuma, K. Ishida, and K. Oikawa, Appl. Phys. Lett. **85**, 4358 (2004).

⁷P. J. Webster, K. R. A. Ziebeck, S. L. Town, and M. S. Peak, Philos. Mag. B **49**, 295 (1984).

⁸V. A. Chernenko, E. Cesari, V. V. Kokorin, and I. N. Vitenko, Scr. Metall. Mater. **33**, 1239 (1995).

⁹K. Ullakko, J. K. Huang, C. Kantner, R. C. O'Handley, and V. V. Kokorin, Appl. Phys. Lett. **69**, 1966 (1996).

¹⁰T. Krenke, E. Duman, M. Acet, E. F. Wassermann, X. Moya, L. Manosa, and A. Planes, Nat. Mater. **4**, 450 (2005).

¹¹T. Krenke, M. Acet, E. F. Wassermann, X. Moya, L. Manosa, and A. Planes, Phys. Rev. B **72**, 014412 (2005).

¹²K. Watanabe, Y. Watanabe, S. Awaji, M. Fujiwara, N. Kobayashi, and T. Hasebe, Adv. Cryog. Eng. **44**, 747 (1998).

¹³P. J. Brown, A. P. Gandy, K. Ishida, R. Kainuma, T. Kanomata, K. U. Neumann, K. Oikawa, B. Oulandiff, and K. R. A. Ziebeck, J. Phys.: Condens. Matter **18**, 2249 (2006).